Effects of high-frequency wind sampling on simulated mixed layer depth and upper ocean temperature

Tong Lee and W. Timothy Liu

Jet Propulsion Laboratory, California Institute of Technology, Pasadena, California, USA

[1] Effects of high-frequency wind sampling on a near-global ocean model are studied by forcing the model with a 12 hourly averaged wind product and its 24 hourly subsamples in separate experiments. The differences in mixed layer depth and sea surface temperature resulting from these experiments are examined, and the underlying physical processes are investigated. The 24 hourly subsampling not only reduces the high-frequency variability of the wind but also affects the annual mean wind because of aliasing. While the former effect largely impacts mid- to high-latitude oceans, the latter primarily affects tropical and coastal oceans. At mid- to high-latitude regions the subsampled wind results in a shallower mixed layer and higher sea surface temperature because of reduced vertical mixing associated with weaker high-frequency wind. In tropical and coastal regions, however, the change in upper ocean structure due to the wind subsampling is primarily caused by the difference in advection resulting from aliased annual mean wind, which varies with the subsampling time. The results of the study indicate a need for more frequent sampling of satellite wind measurement and have implications for data assimilation in terms of identifying the nature of model errors.

Citation: Lee, T., and W. T. Liu (2005), Effects of high-frequency wind sampling on simulated mixed layer depth and upper ocean temperature, *J. Geophys. Res.*, *110*, C05002, doi:10.1029/2004JC002746.

1. Introduction

[2] Ships and buoys do not provide sufficient coverage to monitor global variability of wind forcing of the ocean. Wind field provided by operational numerical weather prediction (NWP) may have deficiency caused by incomplete model physics and inaccurate parameterization. The problem can be mitigated by space-based sensors [*Liu*, 2002]. Satellite scatterometer has been shown to reveal detailed structure of the wind field not resolved by NWP products [*Liu et al.*, 1998]. Yet one instrument with limited swath width on a low polar orbiting satellite may not be sufficient to monitor the temporal variability. The highest resolution scatterometer, i.e., the QuikSCAT mission of the National Aeronautics and Space Administration (NASA), only covers 90% (60%) of the global ocean every 24 (12) hours. Two such scatterometers offset in space and working in tandem can resolve the subdaily variability better as they provide 90% coverage of the global ocean every 12 hours. The main objective of this study is to evaluate the impact of going from 24 hourly to 12 hourly sampling (or vice versa). Previous studies [e.g., *Chen et al.*, 1999; *Sui et al.*, 2003] have examined the difference in the response of the tropical Pacific Ocean to daily versus monthly wind forcing. How-ever, the impact of daily subsampling has not been studied, let alone on the global ocean as a whole.

[3] Specifically, we investigate the response of the upper ocean simulated by a near-global ocean general circulation model (OGCM) to wind products with and without the daily subsampling. Short timescales atmospheric processes affect long-term climate changes through vertical mixing processes at ocean's surface layer as represented by the mixed layer depth (MLD), and ocean's effect on atmospheric changes is manifested through sea surface temperature (SST). Moreover, changes in MLD and SST eventually affect the ocean's thermocline and deeper interior through diffusion. Therefore the present analysis focuses on MLD and SST because of their direct relevance to air-sea interaction and potential impact on the ocean's interior. The oceanic processes that are responsible for the changes in MLD and SST are examined to highlight the physics associated with the response of the model to high-frequency wind forcing.

[4] Section 2 describes the model, the design of the sensitivity experiments, and the impact of the wind subsampling on the variability and annual mean of the wind field. The differences in the oceanic response and the processes responsible for these differences are discussed in section 3. In section 4, the results of the present study are compared with those of previous studies that addressed the impact of high-frequency surface forcing on the tropical Pacific Ocean. Section 5 summarizes the finding. The
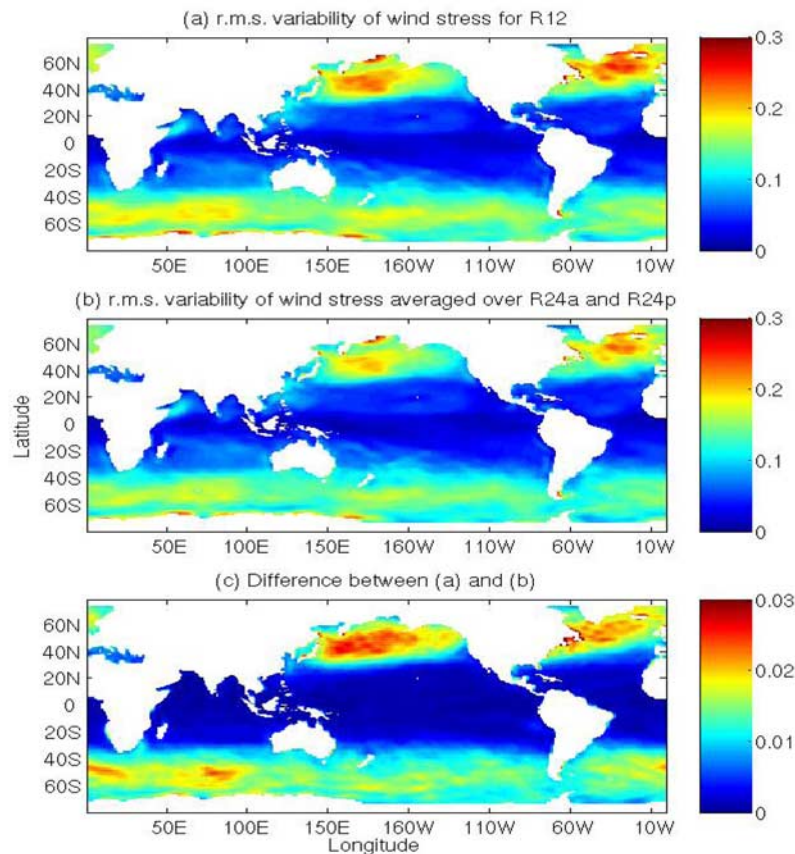
Figure 1. Root-mean-squared variability of the magnitude of wind stress in N/m^2 for (a) R12, (b) the average between R24a and R24p, and (c) their difference. The color scale in Figure 1c is 10 times finer than that in Figures 1a and 1b.

results are not only relevant to the planning of future satellite wind sensors, but important to the physical understanding of the oceanic response to high-frequency wind as well.

2. Model Configuration and Sensitivity Experiments

[5] The model being used is the OGCM of the Massachusetts Institute of Technology [*Marshall et al.*, 1997] as configured by *Lee et al.* [2002]. Briefly, the model domain is global in the zonal direction and spans from 75°S to 75°N meridionally. The horizontal resolution is 1° × 1° poleward of 23°N(S), telescoped to 1° × 0.3° in the tropics. There are 46 vertical levels with a thickness of 10 m in the upper 150 m, gradually increasing to 400 m at depth.

[6] The model employs two advanced mixing schemes: the so-called KPP vertical mixing [*Large et al.*, 1994] and the GM-Redi isopycnal mixing [*Redi*, 1982; *Gent and McWilliams*, 1990]. The model's forcing includes 12 hourly averaged wind stress and daily averaged heat and freshwater fluxes that are interpolated linearly to the hourly time stepping interval of the model integration. These fluxes are based on the reanalysis product of the National Centers for Environmental Prediction (NCEP) and National Center of Atmospheric Research (NCAR) [*Kalnay et al.*, 1996] except that the time averages are replaced by a COADS

product [*da Silva et al.*, 1994]. The NCEP product is also available at 6 hourly averaged intervals, but it is not used in this particular model. In addition to the imposed surface heat and freshwater fluxes, model SST and sea surface salinity are relaxed toward NCEP/NCAR's SST and Levitus'98 climatological mean salinity [*Boyer and Levitus*, 1998], respectively, with timescales of about 1–2 months. After a 10 year spin-up from rest with Levitus'98 climatological temperature and salinity [*Boyer and Levitus*, 1998] forced by seasonal climatological forcings, the model was integrated using the forcings from 1980 to 1999. A more detailed description of the model configuration and comparison of the model state with satellite and in situ data are provided by *Lee et al.* [2002] and *Lee and Fukumori* [2003].

[7] Three experiments are performed to examine the effects of the 24 hourly wind subsampling for year 2000 (the choice for this year is somewhat arbitrary). The control run, R12, uses the default 12 hourly averaged wind, over midnight to noon and noon to midnight, respectively, for Greenwich Mean Time (GMT). The center times are thus 0600 GMT and 1800 GMT, respectively. Two sensitivity runs are performed with a 24 hourly sampling interval. One of these two runs, R24a, uses the 12 hourly sample centered at 0600 GMT. The other run, R24p, uses the 12 hourly sample centered at 1800 GMT. In all three runs, the relaxation of SST and sea surface salinity are turned off to avoid the difference in surface buoyancy input due to the
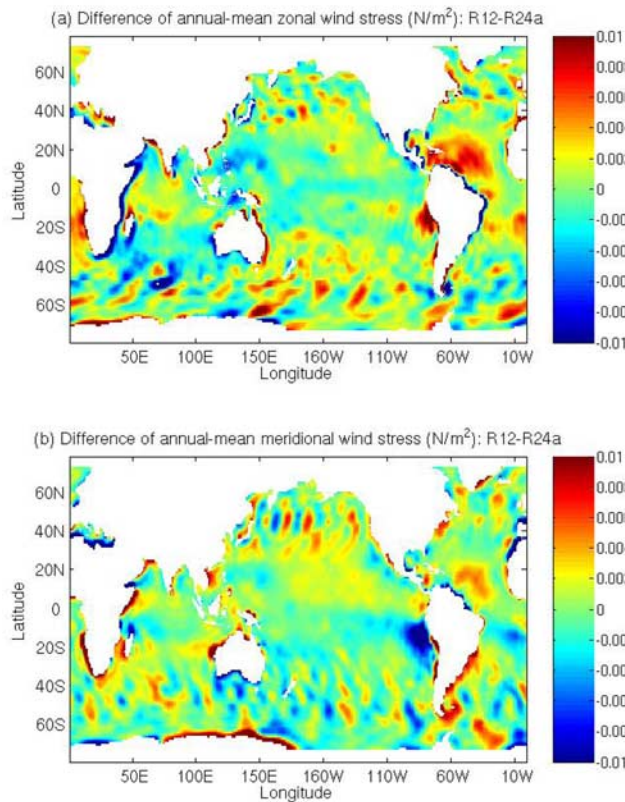
Figure 2. Difference in annual mean (a) zonal and (b) meridional wind stress between R12 and R24a.

relaxation. Therefore any difference among the runs is solely due to the difference in the wind.

[8] The 24 hourly subsampling has two effects on the resultant wind products. First of all, R12 resolves some subdaily variability (despite the 12 hourly average interval) but R24a and R24p do not. Therefore R24a and R24p have weaker high-frequency wind variability than R12. The difference in wind variability between R12 and R24a(p) amounts to about 10% of the total variability in R12 (Figure 1). Secondly, R24a and R24p alias subdaily variability into the annual mean because of the 24 hourly
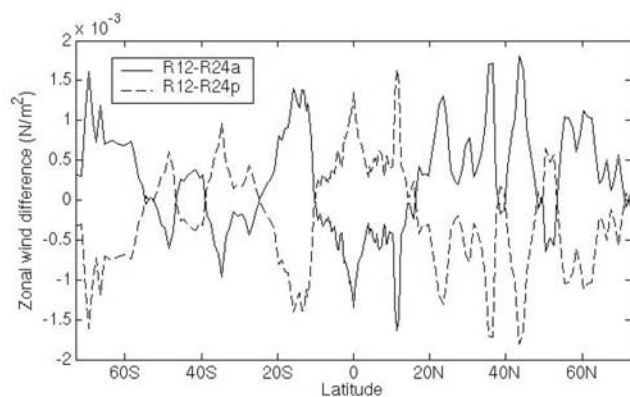

Figure 3. Zonally averaged difference in annual mean zonal wind stress between R12 and R24a (solid curve) and between R12 and R24p (dashed curve).
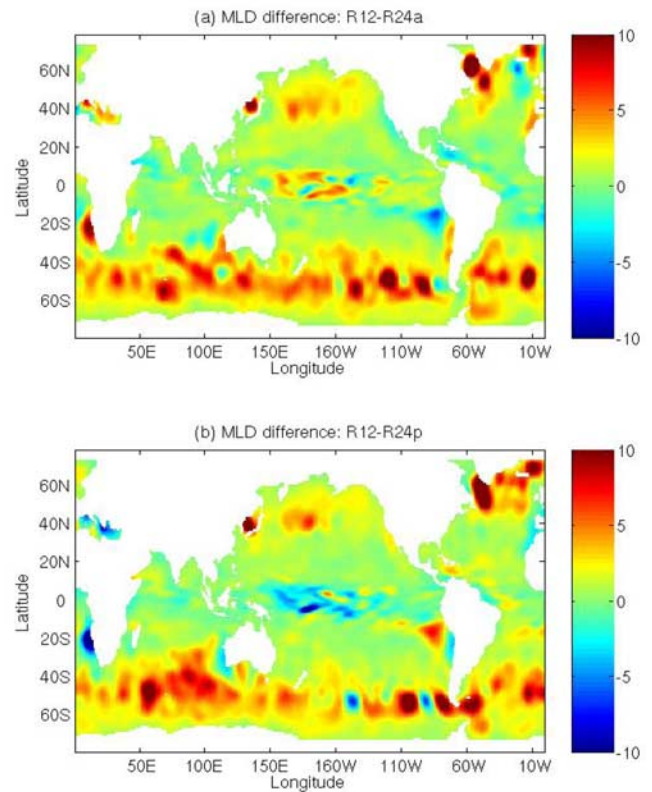

Figure 4. Difference in annual mean mixed layer depth (in meters) (a) between R12 and R24a and (b) between R12 and R24p.

subsampling. The aliases of R24a and R24p wind are different because of the difference in subsampling time. Figure 2 shows the differences in annual mean zonal and meridional wind stress between R12 and R24a. The corresponding differences between R12 and R24p are not shown because they are opposite in sign to Figure 2. The zonally averaged difference of annual mean zonal wind between R12 and R24a and that between R12 and R24p are shown in Figure 3.

[9] The differences seen in Figures 2 and 3 are purely due to the aliasing of subdaily variability into the annual mean. In Figure 2, the wave-like patterns over mid- to high-latitude oceans reflect the aliasing of synoptic weather features. Therefore the resultant difference in zonal average (Figure 3) at these latitudes reflects the phase distortion of weather systems rather than the difference in large-scale wind. Near many coastal regions (e.g., off the east coasts of Africa and Australia), the aliasing is due to the subsampling of the (diurnal) sea breeze. In the tropics, the scale of the differences resulted from the subsampling is relatively large. This is believed to be associated with the aliasing of large-scale atmospheric thermal tides on diurnal and semidiurnal timescales as discussed by *Desser* [1994] and *Dai and Deser* [1999].

[10] The 12 hourly versus 24 hourly sampling has some relevance to space-borne wind measurement. As mentioned before, QuikSCAT has a 24 hourly sampling rate over much of the global ocean. Two such scatterometers working in tandem would increase the sampling rate to every 12 hours.
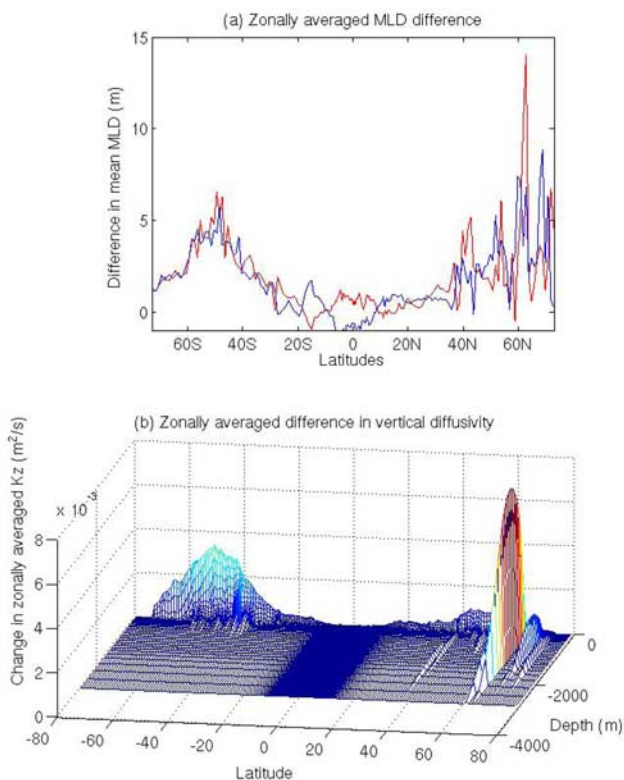
Figure 5. Zonally averaged difference in annual mean (a) mixed layer depth between R12 and R24a (red curve) and between R12 and R24p (blue curve) and (b) vertical diffusivity between R12 and the average of R24a and R24p. The colors in Figure 5b are only for visualization purposes and have no physical meaning.

The sampling times of QuikSCAT's ascending and descending tracks (0600 and 1800 LT, respectively) are different from the subsampling times of R24a and R24p wind (0600 and 1800 GMT). However, before the satellite track data are used to force an ocean model, they are usually interpolated in space and time to a regular grid with each map centered at a specific GMT. For example, 24 hourly maps of wind stress can be generated from the QuikSCAT data as the satellite covers 90% of the global ocean every 24 hours. In a loose sense, the subsampling for R24a(p) is somewhat analogous to the 24 hourly sampling of gridded QuikSCAT maps of wind stress. The wind field measured by one scatterometer would have less high-frequency variability than that measured by two scatterometers, and that it would have alias of high-frequency wind into the annual mean (although the alias depends on the sampling time). The processes responsible for the difference in oceanic response to the 12 hourly and 24 hourly NCEP wind products would help understand the different impact of one versus two QuikSCAT-like scatterometers.

3. Results

[11] Let H denote the annually averaged (over year 2000) mixed layer depth (MLD), defined here as the depth at which the temperature is lower than SST by 0.5°C, a commonly used threshold [e.g., *Kessler et al.*, 1998; *Wang*

and McPhaden, 1999]. An alternative definition of MLD based on density increment does not alter the conclusions of this study. Figure 4a shows the differences in H between R12 and R24a and between R12 and R24b, i.e., $H(R12) - H(R24a)$ (panel a) and $H(R12) - H(R24p)$ (panel b). In mid- to high-latitude oceans, $H(R12)$ is generally larger than $H(R24a)$ and $H(R24p)$. The wave-like features of $H(R12) - H(R24a)$ and $H(R12) - H(R24p)$ in these regions are most likely caused by the distortion of weather patterns and the aliasing into annual mean wind of R24a(p) (e.g., Figure 2).

[12] The zonally averaged MLD differences $\overline{H}(R12) - \overline{H}(R24a)$ and $\overline{H}(R12) - \overline{H}(R24p)$ (where an overbar represents zonal average) are shown in Figure 5a. Again, the positive values at middle- to high-latitude oceans clearly suggest that the MLD is larger in R12 than in R24a(p). Our analysis shows that this is associated with larger vertical mixing in R12 induced by stronger high-frequency wind. To illustrate this point, we present in Figure 5b the meridional-vertical distribution of the zonally averaged difference in annual mean vertical diffusive coefficient between R12 and R24a(p), $[\overline{\kappa}(R12) - \overline{\kappa}(R24a) + \overline{\kappa}(R12) - \overline{\kappa}(R24p)]/2$ (where $\overline{\kappa}$ is zonally averaged annual mean vertical diffusivity). The generally positive values of this quantity at mid- to high-latitude upper oceans reflect the larger variability of high-frequency wind in R12 in these regions as seen in Figure 1c.
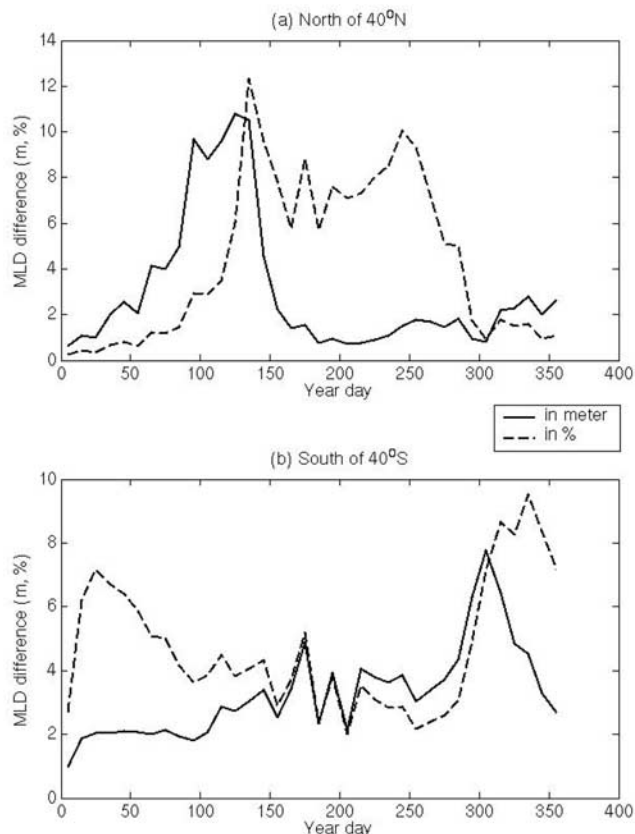

Figure 6. Seasonal distribution of the difference (solid curves) and percentage difference (dashed curves) in mixed layer depth averaged over high-latitude oceans (a) north of 40°N and (b) south of 40°S.
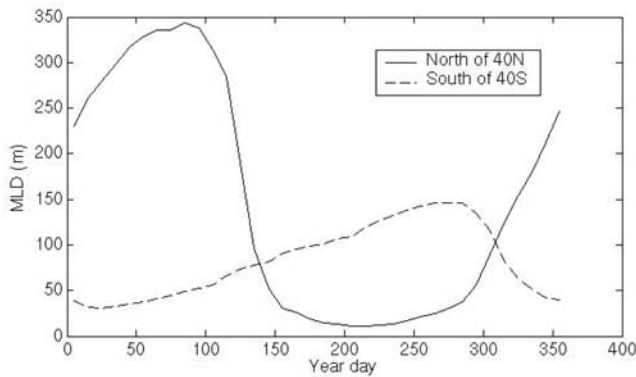
Figure 7. Seasonal variation of mixed layer depth for the control run R12 averaged over the oceans north of 40°N and south of 40°S.

[13] While the MLD at mid- and high-latitude oceans is generally larger with the more frequently sampled wind (R12), that at tropical and coastal oceans is not. In the latter regions, the signs of $H(R12) - H(R24a)$ and $H(R12) - H(R24p)$ are generally opposite to each other (Figure 4). Such a behavior cannot be explained by vertical mixing because the difference in vertical diffusivity between R12 and R24a(p) is very small in these regions (see Figure 5b for the tropical case). As will be discussed later on in this
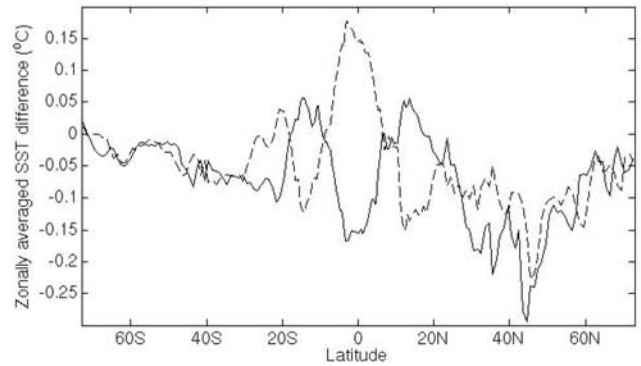

Figure 9. Zonally averaged differences in annual mean SST between R12 and R24a and between R12 and R24p.

section, the dominant process responsible for the changes in upper ocean structure in tropical and coastal oceans is advection, which depends on the annual mean wind.

[14] The response of MLD at mid- to high-latitude oceans to high-frequency wind varies with season. The solid curves in Figure 6 show the seasonal variation of MLD difference $[H(R12) - H(R24a) + H(R12) - H(R24p)]/2$ averaged over the oceans north of 40°N (panel a) and South of 40°S (panel b). In both hemispheres, the largest change of this quantity occurs in the respective springtime. However, the season that has large change does not necessarily coincide with the season that has large percentage change. The percentage change in MDL, $[H(R12) - H(R24a) + H(R12) - H(R24p)]/[2H(R12)]$, is shown by the dashed curves in Figure 6. During summertime, the change in MLD is relatively small but the percentage change is relatively large. This is because the MLD itself is small during summertime (Figure 7) so a small change in MLD corresponds to a large percentage change.
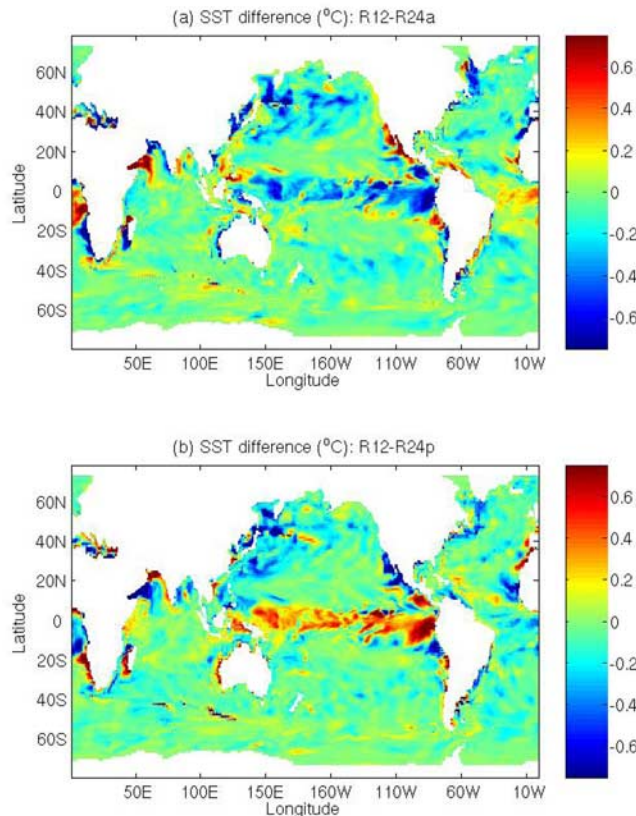

Figure 8. Difference in annual mean sea surface temperature (SST) (a) between R12 and R24a and (b) between R12 and R24p.
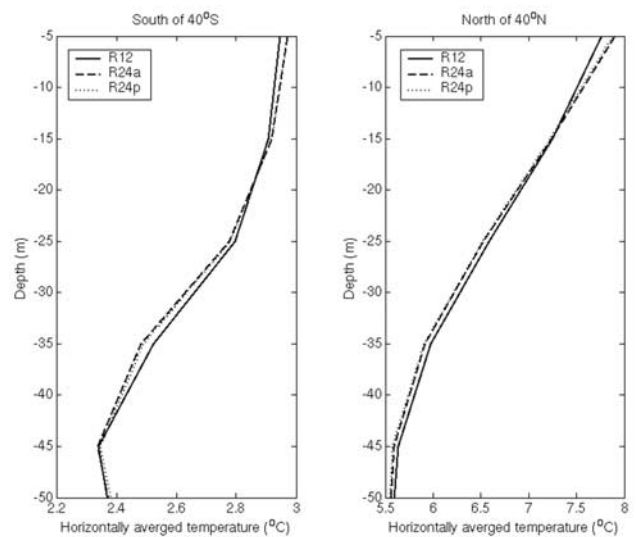

Figure 10. Vertical profile of temperature averaged over high-latitude oceans north of 40°N and south of 40°S for R12 (solid curve), R24a (dashed curve), and R24p (dash-dotted curve).
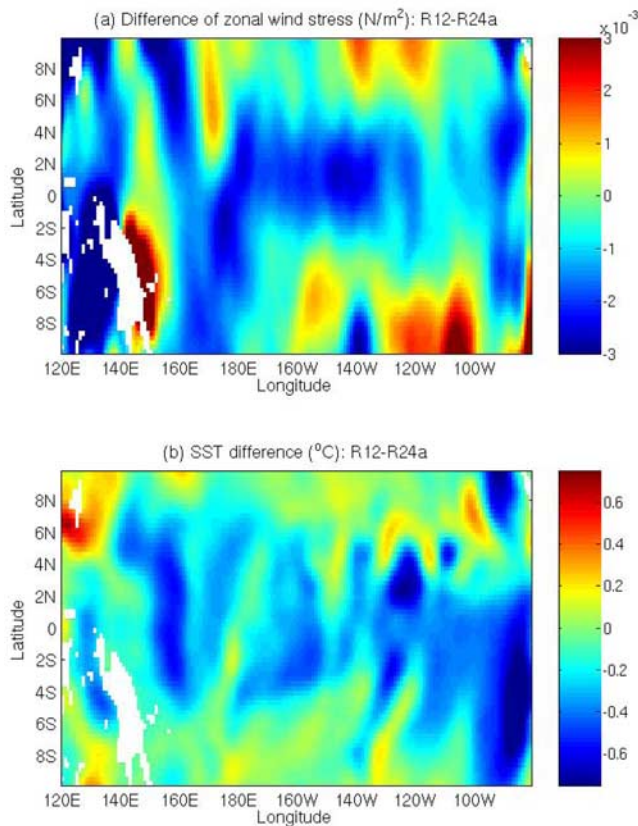
Figure 11. Difference in annual mean (a) zonal wind stress and (b) SST between R12 and R24a in the tropical Pacific.

Figure 13. Zonal sections of the difference in annual mean temperature at (a) the equator, (b) 5°N, and (c) 5°S between R12 and R24a.

[15] We now proceed to the discussion of the difference in upper ocean temperature, focusing on SST. Figure 8 shows the difference in annual mean SST between R12 and R24a (panel a) and that between R12 and R24p (panel b). The corresponding zonal averages are shown in Figure 9 by the solid and dashed curves, respectively. At mid- to high-latitude oceans, SST is generally lower in R12 (Figure 9), consistent with the stronger vertical mixing in this case as discussed earlier. To strengthen this point, the
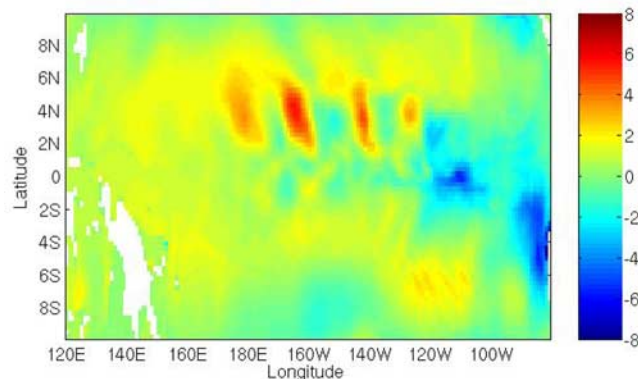

Figure 12. Difference in annual mean thermocline depth (using the depth of 18°C isotherm as a proxy) between R12 and R24a.
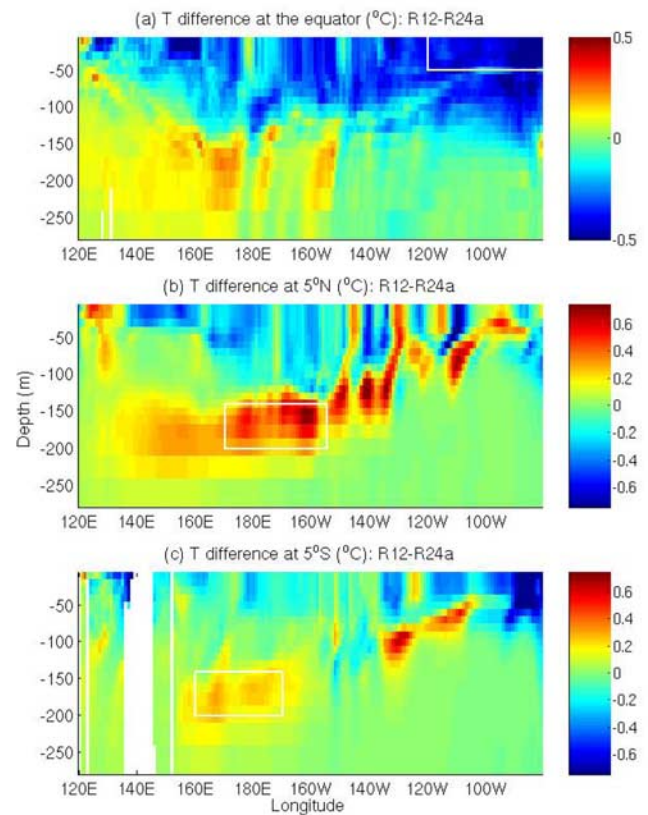
vertical profiles of temperature averaged over high-latitude oceans north of 40°N and south of 40°S are shown in Figure 10 for all three runs. Owing to the stronger vertical mixing in R12, the near-surface stratification for this run (solid curve) is weaker than that for R24a and R24p (dashed and dash-dotted curves).

[16] As seen from Figure 3, the 24 hourly subsampling results in different signs of aliasing into the annual mean wind for R24a and R24p at most latitudes. This is expected to affect the annual mean upper ocean currents and thus the heat advection. The consistently shallower mixed layer and higher SST at mid- to high-latitude oceans for R24a and R24p suggest that advection is not as important as vertical mixing in these regions. However, as discussed in the following, the opposite is true for tropical and coastal oceans.

[17] In tropical and coastal regions, the difference in SST between R12 and R24a and that between R12 and R24p are generally opposite in sign to each other (Figures 8 and 9). As substantiated in the following, the dominant process affecting upper ocean changes in these regions is the advection resulted from the aliased annual mean wind (e.g., Figure 3). The difference in SST between R12 and R24a in the tropical Pacific is generally negative in the equatorial zone. The magnitude of the difference is about 0.5°C in the eastern equatorial Pacific. This is substantial because it is comparable to the usual threshold for defining the SST anomaly associated with an El Niño. To illustrate

Table 1. Total Difference in Temperature and the Breakdown of Contribution by Advection and Diffusion Averaged Over Three Regions in the Equatorial Pacific

Region (Equatorial Pacific)	Total Temperature Change, °C	Advection	Diffusion
120°−80°W, 2°S−2°N (0−50 m)	−0.49	−0.41	−0.09
170°E−155°W, 4°−6°N (140−200 m)	0.58	0.66	−0.08
160°E−170°W, 4°−6°S (140−200 m)	0.21	0.29	−0.08

the dominant role of heat advection, the difference in zonal wind and SST between R12 and R24a are replotted for the tropical Pacific (Figure 11). A finer color scale is used in Figure 11a (comparing to that in Figure 2a) to allow a better visualization of the aliased wind over the equatorial Pacific. R12 has a stronger equatorial easterly trade than R24a (blue color near the equator in Figure 11a). As a result, R12 has a more westward surface current near the equator and a stronger upwelling in the eastern equatorial Pacific. The stronger eastern upwelling and larger westward advection of cold tongue water both contribute to the lower SST in R12 (Figure 11b). The banded pattern in the zonal direction appears to be due to the distortion of the phase of tropical instability waves in R24a.

[18] The difference of annual mean wind between R12 and R24a also causes an uplift of the thermocline in the eastern equatorial Pacific and a depression in the western equatorial Pacific as well as off the equator (Figure 12). The zonal sections of temperature difference between R12 and R24a at the equator, 5°N, and 5°S are shown in Figure 13. The higher temperature near the thermocline (around the depths of 150−200 m, shallower toward east) in the western part of the equator and at 5°N and 5°S illustrate the consequence of the thermocline depression.

[19] To quantify the role of advection, the differences in total temperature tendency and in the advective and diffusive contributions between R12 and R24a for the three boxes shown in Figure 13 are listed in Table 1. Indeed, the advective contribution accounts for most of the temperature difference. The results of a similar analysis for three coastal regions (near the Red Sea and Somalia coast, off the west coast of America, and southwest of Madagascar) are also presented (Table 2). Again, the advection is the major cause for the temperature difference in all three coastal regions. Therefore both for tropical and coastal oceans, the difference in oceanic advection due to the aliased annual mean wind plays a leading role in causing the differences in upper ocean temperature structure among different experiments.

[20] The present study uses the NCEP/NCAR wind product and its 24 hourly subsamples to evaluate the impact of the subsampling on the OGCM. An important issue is whether the subdaily variability of the NCEP/NCAR wind is representative of actual observations at all. To address this issue, we compare the subdaily variation of the NCEP wind during year 2000 with the composite diurnal wind obtained

from the TAOGA-TAO moorings during the same period. Some qualitative agreement is found. As an example, the composite diurnal anomaly of zonal wind from the TAO mooring at 170°W at the equator is shown in Figure 14 (the time axis is referenced to the GMT). The 12 hourly average centered at 0600 is about 0.001 N/m^2 more positive than the mean (which has been removed in the figure). In other words, the difference between the mean and this 12 hourly average is about −0.001 N/m^2. This is more or less consistent with the NCEP/NCAR product (Figure 11a).

[21] The sensitivity experiments are only done for year 2000. The differences between the control and sensitivity experiments may increase with time until equilibrium is reached in all runs. Extended integration is needed for all the runs in order to assess the equilibrium time limit. It is not clear whether this would require years or decades (or even longer). A much longer integration allows for an assessment of the impact of wind subsampling on interannual and decadal variability. While these are interesting questions, they are beyond the scope of this study that focuses on the tendency of the annual mean difference and the underlying processes.

[22] In OGCM simulations, the model's SST and sea surface salinity are often relaxed toward the corresponding observations to prevent the model from drifting. As mentioned in section 2, we purposely turn off the relaxation to isolate the wind effect. Nevertheless, a question remains as to whether one would still see these differences were the relaxation applied. We have performed the corresponding experiments with the relaxation turned on (having a time-scales of 1−2 months). The differences in MLD and SST due to the subsampling are approximately 50% of those without the relaxation. We choose not to discuss these experiments here because the surface buoyancy fluxes are not identical due to the artificial relaxation fluxes, precluding the isolation of the wind effect.

4. Comparisons With Previous Studies

[23] The impacts of high-frequency surface forcing on the tropical Pacific Ocean have been investigated before [*Chen et al.*, 1999; *Sui et al.*, 2003]. *Chen et al.* [1999] examined the response of a tropical Pacific Ocean model to temporal smoothing in wind stress from 1 to 30 days during the onset of the 1997−1998 El Niño. It was found that the SST

Table 2. Total Difference in Temperature and the Breakdown of Contribution by Advection and Diffusion Averaged Over Three Coastal Regions

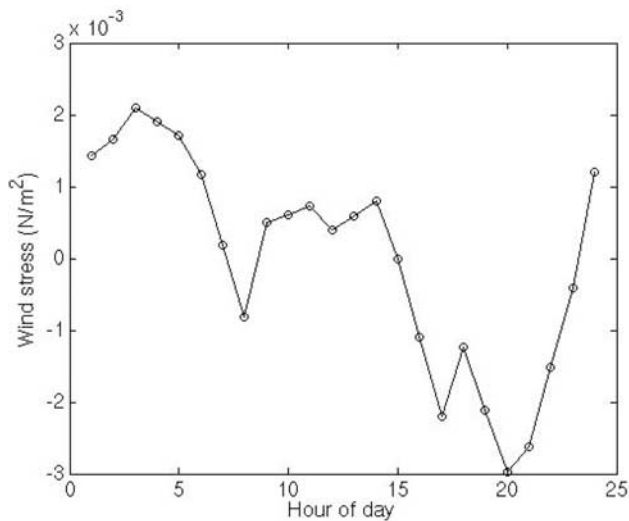| Region (Coastal Oceans)	Total Temperature Change, °C	Advection	Diffusion
43°−63°E, 10°−18°N, 0−50 m (Red Sea, Somali)	0.66	0.59	0.07
120°−105°W, 18°−34°N, 0−50 m (off west coast of America)	0.55	0.66	−0.11
40°−46°E, 20°−30°S, 0−50 m (southwest of Madagascar)	−1.19	−1.44	0.25

Figure 14. Averaged diurnal cycle of zonal wind stress as measured by the TOGA-TAOI mooring at 170°W, 0°N during year 2000.

generally became higher as the smoothing interval increased because the reduced vertical mixing associated with the smoother wind trapped more energy input in the upper layer. *Sui et al.* [2003] contrasted the response of their Pacific Ocean model to daily and monthly forcing. The equatorial Pacific Ocean was also found to be warmer with the monthly forcing than with the daily forcing. In the eastern equatorial Pacific, the major cause for the difference in SST was zonal advection. However, the difference in the surface current was due to the difference in mixing that modified the vertical shear.

[24] There are several major differences between the present study and the two previous efforts apart from the domain of interest (tropical Pacific in the previous studies and global ocean for the present study). First of all, the present study focuses on the impact of 12 hourly versus 24 hourly wind sampling whereas the previous studies addressed daily versus and longer-period (e.g., monthly) forcing to evaluate the impact of transient weather. The response to the forcing and the underlying processes could vary with timescales. Secondly, the lower-frequency forcing used in the present study was obtained by 24 hourly subsampling, not 24 hourly average. As discussed in section 2, this causes a bias in annual mean wind because of aliasing, which affects the circulation. However, the lower-frequency forcings used in the previous studies were obtained through averaging or temporal smoothing that introduced no bias in the annual mean forcing. Although *Sui et al.* [2003] also found advection to be the leading cause for SST difference in the eastern equatorial Pacific, the fundamental cause of the change in the currents was the change in mixing due to wind variability, not the aliased annual mean wind discussed in the present study.

[25] Finally, the surface flux formulations are not all the same among these studies. Like the present study, *Chen et al.* [1999] isolated the effect of different wind products by using the same buoyancy flux in different experiments. However, *Sui et al.* [2003] used a diagnostic atmospheric boundary layer flux formulation that included some level of

interaction between SST and air-sea fluxes. The process responsible for the difference in the response to high-frequency wind may depend on the flux formulation. Ideally, the investigation of the physics associated with oceanic response to atmospheric forcing should be done with a fully coupled ocean-atmosphere model instead of a forced ocean model (regardless of the surface flux formulation). However, studies with forced ocean models are still useful in many contexts, for instance, to evaluate the impact of wind subsampling or smoothing on the ocean simulation.

5. Concluding Remarks

[26] The impact of high-frequency wind sampling on a near-global OGCM is investigated by forcing the model with 12 hourly averaged NCEP/NCAR reanalysis wind and its 24 hourly subsamples in different experiments. The resultant solutions are compared, focusing on the differences in mixed layer depth and sea surface temperature as well as the processes that are responsible for these differences. The 24 hourly subsampling exerts two types of influence on the resultant wind: a reduction of high-frequency variability because of the exclusion of subdaily variation, and a biased annual mean due to aliasing. These two effects primarily influence mid- to high-latitude oceans and tropical and coastal oceans, respectively.

[27] At mid- and high-latitude regions, the 24 hourly subsampled wind results in a shallower mixed layer and higher sea surface temperature due to less vertical mixing associated with weaker high-frequency wind. In tropical and coastal regions, the change in upper ocean structure is primarily due to the difference in advection associated with aliased annual mean wind, which depends on the subsampling time.

[28] Of all the tropical oceans, the eastern equatorial Pacific displays the largest difference in SST (about 0.5°C) due to the wind subsampling. This difference is reduced by about 50% when model SST is relaxed toward observed values. Since the original difference is caused by the wind, the relaxation imposes an incorrect process by artificially creating a surface heat flux. This has implications to the assimilation of SST data in ocean model where the errors of wind and surface heat flux need to be prescribed appropriately. The results of this study also indicate a need to increase the temporal sampling of spaced-based wind sensors.

References

Boyer, T. P., and S. Levitus (1998), Objective analysis of temperature and salinity for the world ocean on a 1/4° grid, *World Ocean Atlas 1998*, *NOAA Atlas NESDIS 11*, pp. 1–62, Natl. Oceanic and Atmos. Admin., Silver Spring, Md.

Chen, D., W. T. Liu, S. E. Zebiak, M. A. Cane, Y. Kushnir, and D. Witter (1999), Sensitivity of the tropical Pacific Ocean simulation to the temporal and spatial resolution of wind forcing, *J. Geophys. Res.*, *104*, 11,261–11,271.

Dai, G., and C. Deser (1999), Diurnal and semidiurnal variations in global surface wind and divergence fields, *J. Geophys. Res.*, *104*, 31,109–31,125.

da Silva, A., A. C. Young, and S. Levitus (1994), *Atlas of Surface Marine Data*, *NOAA Atlas NESDIS 6*, U.S. Dept. of Commerce, Washington, D. C.

Desser, C. (1994), Daily surface wind variations over the equatorial Pacific Ocean, *J. Geophys. Res.*, *99*, 23,071–23,078.

Gent, P., and J. McWilliams (1990), Isopycnal mixing in ocean circulation models, *J. Phys. Oceanogr.*, *20*, 150–155.

Kalnay, E., et al. (1996), The NCEP/NCAR 40-year reanalysis project, *Bull. Am. Meteorol. Soc.*, *77*, 437–471.

Kessler, W. S., L. M. Rothstein, and D. Chen (1998), The annual cycle of SST in the eastern tropical Pacific, diagnosed in an ocean GCM, *J. Clim.*, *11*, 777–799.

Large, W. G., J. C. McWilliams, and S. C. Doney (1994), Oceanic vertical mixing: A review and a model with a nonlocal boundary layer parameterization, *Rev. Geophys.*, *32*, 363–403.

Lee, T., and I. Fukumori (2003), Interannual-to-decadal variations of tropical-subtropical exchange in the Pacific Ocean: Boundary versus interior pycnocline transports, *J. Clim.*, *16*, 4022–4042.

Lee, T., I. Fukumori, D. Menemenlis, Z. Xing, and L.-L. Fu (2002), Effects of the Indonesian throughflow on the Pacific and Indian Oceans, *J. Phys. Oceanogr.*, *32*, 1404–1429.

Liu, W. T. (2002), Progress in scatterometer applications, *J. Oceanogr.*, *58*, 121–136.

Liu, W. T., W. Tang, and P. S. Polito (1998), NASA scatterometer provides global ocean-surface wind fields with more structures than numerical weather prediction, *Geophys. Res. Lett.*, *25*, 761–764.

Marshall, J., A. Adcroft, C. Hill, L. Perelman, and C. Heisey (1997), A finite-volume, incompressible Navier Stokes model for studies of the ocean on parallel computers, *J. Geophys. Res.*, *102*, 5753–5766.

Redi, M. (1982), Oceanic isopycnal mixing by coordinate rotation, *J. Phys. Oceanogr.*, *12*, 1154–1157.

Sui, C. H., X. F. Li, M. M. Rienecker, K. M. Lau, I. Laszlo, and R. T. Pinker (2003), The role of daily surface forcing in the upper ocean over the tropical Pacific: A numerical study, *J. Clim.*, *16*, 756–766.

Wang, W. M., and M. J. McPhaden (1999), The surface-layer heat balance in the equatorial Pacific Ocean. part I: Mean seasonal cycle, *J. Phys. Oceanogr.*, *29*, 1812–1831.

_____

T. Lee and W. T. Liu, Jet Propulsion Laboratory, California Institute of Technology, 4800 Oak Grove Drive, Pasadena, CA 91109, USA. (tlee@pacific.jpl.nasa.gov; liu@pacific.jpl.nasa.gov)